

Metal-organic framework-modified separator enables long cycling lithium-ion capacitors with asymmetric electrolyte design

Yunlong Zhang,^a Yanan Li,^a Xiaoshan Wang,^a Xiaoling Teng,^a Lu Guan,^a Hao Yang,^a Yi Wan,^a Shiwei Guo,^a Han Hu,^{*a} and Mingbo Wu^{*a}

^aState Key Laboratory of Heavy Oil Processing, Institute of New Energy, College of Chemistry and Chemical Engineering, China University of Petroleum (East China), Qingdao 266580, China.

Contents:

Figure S1. XRD characterization of as-synthesized ZIF-7 particles.

Figure S2. (a) SEM image of the as-synthesized ZIF-7 particles. (b) Cross-sectional SEM image of a ZIF-7 modified glass fiber separator.

Figure S3. The dimension of I_3^- species.

Figure S4. CV curves of the cell using the AC cathode at the scan rate of 0.5 mV/s of different cycles.

Figure S5. SEM image of the ZIF-7 particles after long-term cycling.

Figure S6. SEM image of (a) fresh surface of a lithium foil. SEM images of the cycled lithium foil surface from the cell using the traditional separator (b) and ZIF-7 modified separator.

Figure S7. CV curves of the cell using the AC cathode at different scan rates.

Figure S8. (a) XRD and (b) SEM characterization of as-synthesized $3DC@Li_2TiSiO_5$ powder.

Figure S9. Electrochemical performance test of $3DC@Li_2TiSiO_5$. (a) CV curves, (b) GCD profiles, (c) rate performance, and (d) cyclic capability of $3DC@Li_2TiSiO_5$. The insert curve in (d) is GCD profile of the 1500th cycle.

Figure S10. Schematic illustration of dual ion adsorption of the AC cathode at 0.1 A g^{-1} .

Figure S11. CV curves of AC// $3DC@Li_2TiSiO_5$ LICs with traditional and ZIF-7 modified separators after several cycles.

Table S1. Comparison of electrochemical performance of lithium ion capacitors.

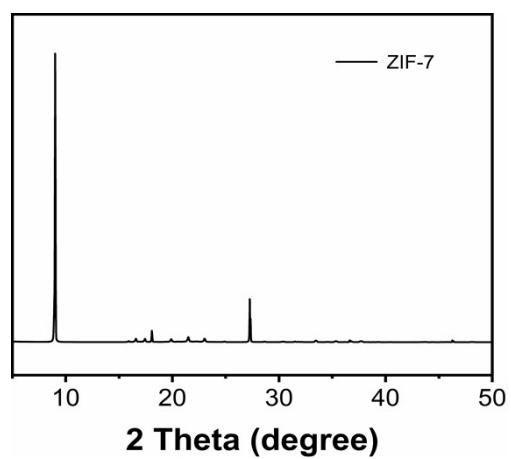


Figure S1. XRD characterization of as-synthesized ZIF-7 particles.

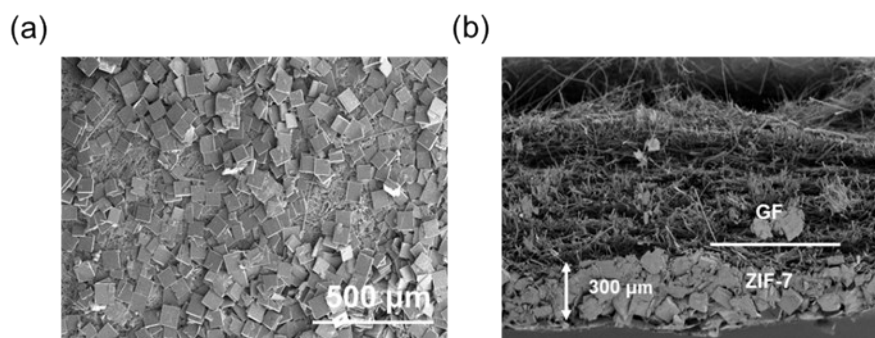


Figure S2. (a) SEM image of the as-synthesized ZIF-7 particles. (b) Cross-sectional SEM image of a ZIF-7 modified glass fiber separator.

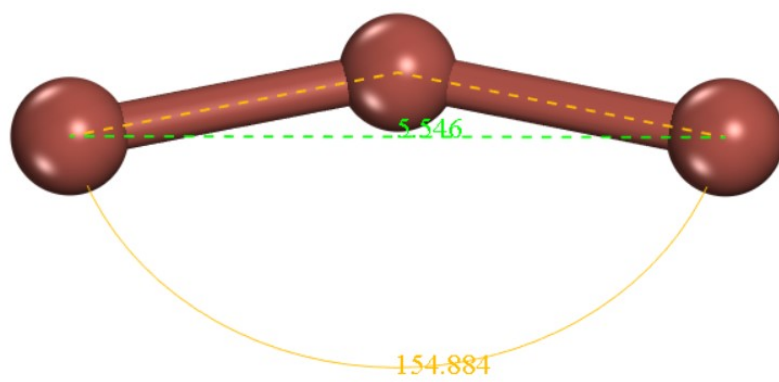


Figure S3. The dimension of I_3^- species.

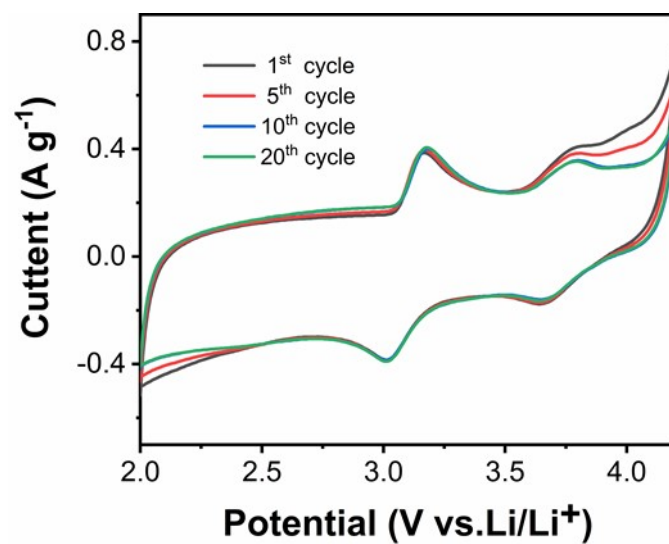


Figure S4. CV curves of the cell using the AC cathode at the scan rate of 0.5 mV/s of different cycles.

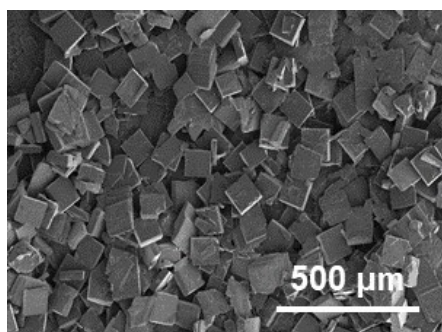


Figure S5. SEM image of the ZIF-7 particles after long-term cycling.

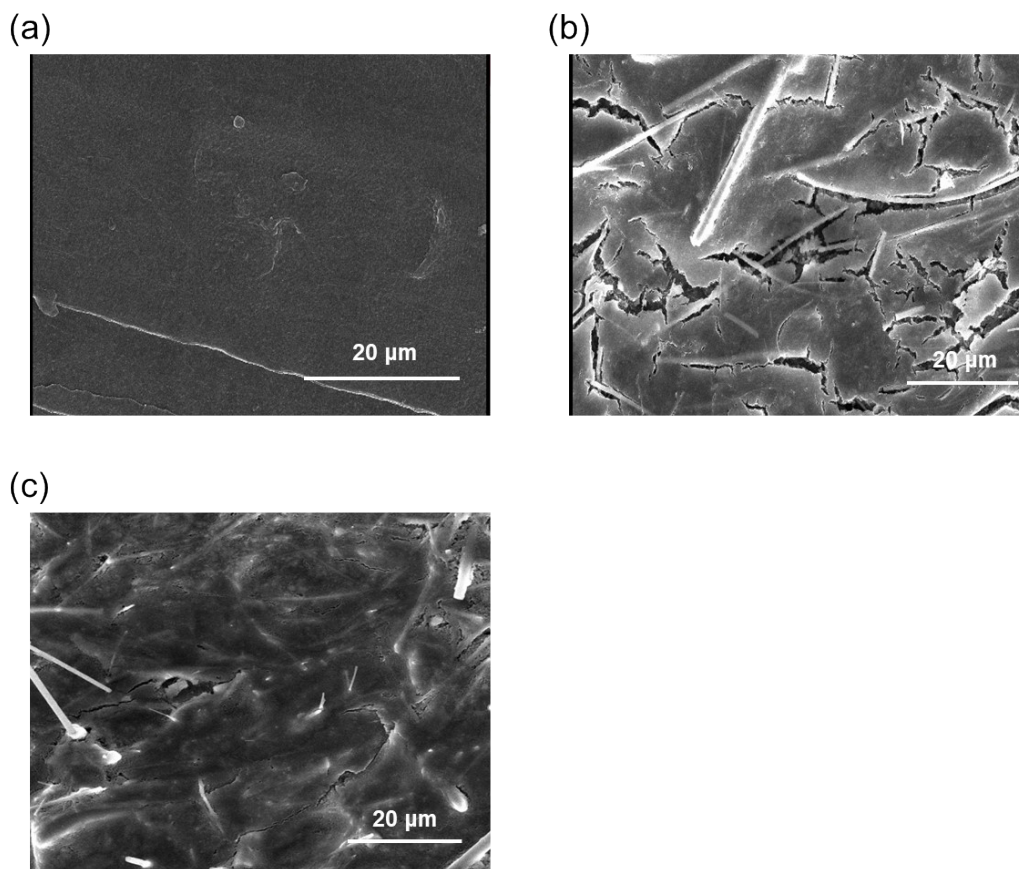


Figure S6. SEM image of (a) fresh surface of a lithium foil. SEM images of the cycled lithium foil surface from the cell using the traditional separator (b) and ZIF-7 modified separator.

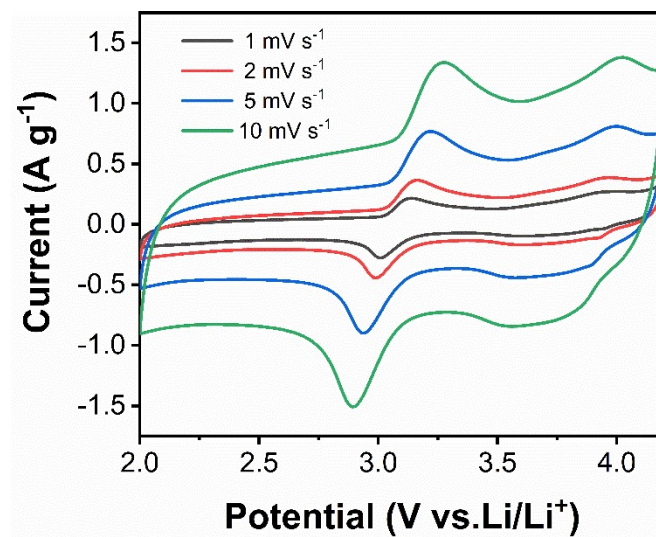


Figure S7. CV curves of the cell using the AC cathode at different scan rates.

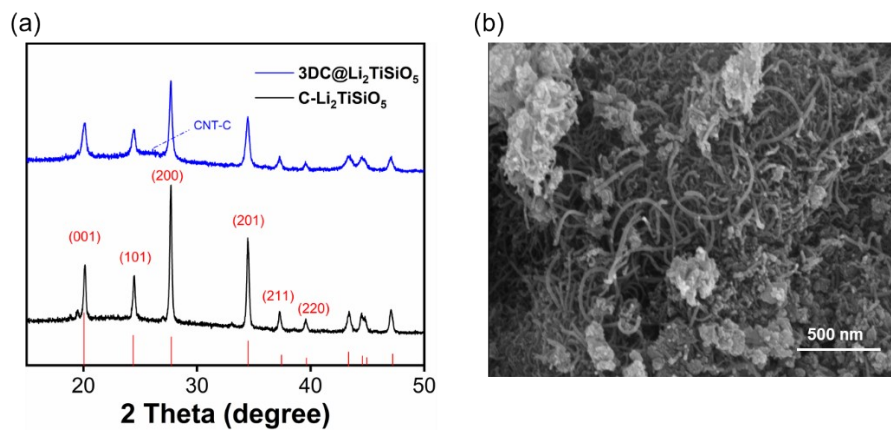


Figure S8. (a) XRD and (b) SEM characterization of as-synthesized 3DC@Li₂TiSiO₅ powder.

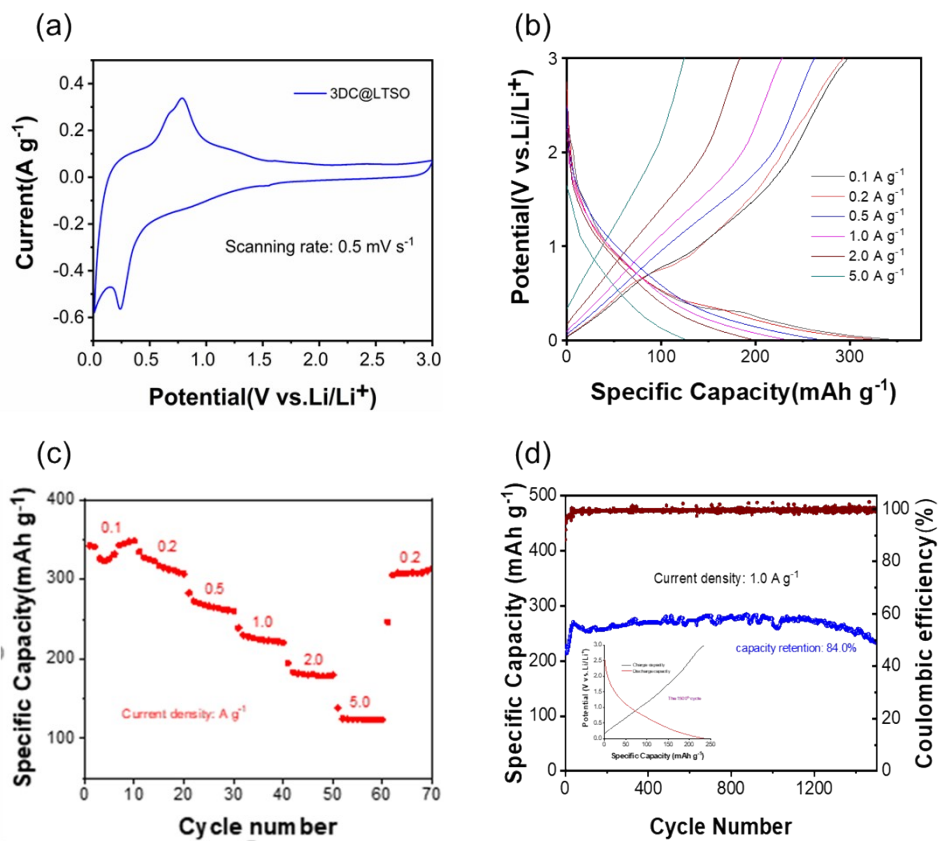


Figure S9. Electrochemical performance test of 3DC@Li₂TiSiO₅. (a) CV curves, (b) GCD profiles, (c) rate performance, and (d) cyclic capability of 3DC@Li₂TiSiO₅. The insert curve in (d) is GCD profile of the 1500th cycle.

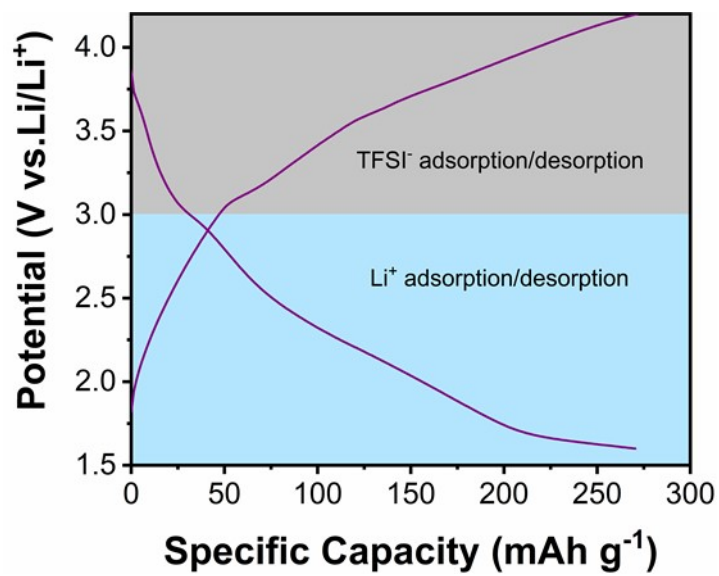


Figure S10. Schematic illustration of dual ion adsorption of the AC cathode at 0.1 A g⁻¹.

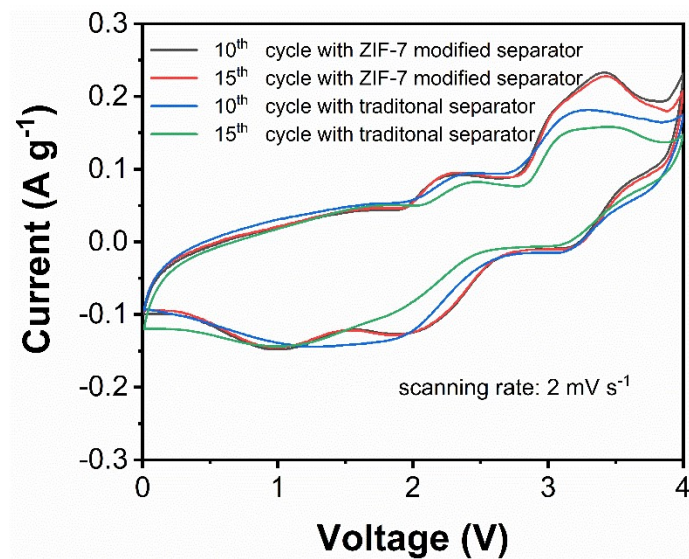


Figure S11. CV curves of AC//3DC@Li₂TiSiO₅ LICs with traditional and ZIF-7 modified separators after several cycles.

Table S1 Comparison of electrochemical performance of lithium ion capacitors.

Anode	Cathode	Energy Density (Wh kg ⁻¹)	Cycling Number	Capacity Retention	Ref.
SnO ₂	rGO	186	5000	70 %	[1]
Li ₃ VO ₄	AC	136.4	1500	87 %	[2]
CNT@ pLTO	GF	101.8	5000	84.8 %	[3]
Zr-MOF	AC	122.5	1000	86 %	[4]
graphite	AC	162.3	-	-	[5]
PHC	AC	104	5000	84.7 %	[6]
NPCM-A	MoS ₂ /N- NPCM	120	4000	85.5 %	[7]
Li ₅ ReO ₆	AC	40	5000	-	[8]
G-LTO	graphene- sucrose	95	500	94 %	[9]
LTSO	AC+LiI	238.56	4000	85.2 %	This work

References

- [1] J. Ajuria, M. Arnaiz, C. Botas, D. Carriazo, R. Mysyk, T. Rojo, A.V. Talyzin, E. Goikolea. Graphene-based lithium ion capacitor with high gravimetric energy and power densities. *Journal of Power Sources*, 2017, (363): 422-427.
- [2] L. Shen, H. Lv, S. Chen, P. Kopold, P.A. Aken, X. Wu, J. Maier, Y. Yu, Peapod-like Li₃VO₄/N-Doped Carbon Nanowires with Pseudocapacitive Properties as Advanced Materials for High-Energy Lithium-Ion Capacitors. *Advanced Materials*. 2017: p. 1700142.
- [3] Y. Liu, W. Wang, J. Chen, X. Li, Q. Cheng, G. Wang, Fabrication of porous lithium titanate self-supporting anode for high performance lithium-ion capacitor. *Journal*

- of Energy Chemistry 2020, (50): 344–350.
- [4] W. Yan, J. Su, Z. Yang, S. Lv, Z. Jin, J. Zuo, High-Performance Lithium-Ion Capacitors Based on Porosity-Regulated Zirconium Metal-Organic Frameworks. *Small* 2020: p. 2005209.
- [5] P. Sennu, V. Aravindan, M. Ganesan, Y. Lee, Y. Lee, Biomass-Derived Electrode for Next Generation Lithium-Ion Capacitors. *ChemSusChem* 2016, (9): 849 – 854.
- [6] Z. Yang, Y. Gao, Z. Zhao, Y. Wang, Y. Wu, X. Wang, Phytic acid assisted formation of P-doped hard carbon anode with enhanced capacity and rate capability for lithium ion capacitors. *Journal of Power Sources* 2020, (474): p. 228500.
- [7] J. Jiang, Y. Zhang, Y. An, L. Wu, Q. Zhu, H. Dou, X. Zhang, Engineering Ultrathin MoS₂ Nanosheets Anchored on N-Doped Carbon Microspheres with Pseudocapacitive Properties for High-Performance Lithium-Ion Capacitors. *Small Methods* 2019: p. 1900081.
- [8] P. Jeżowska, K. Fic, O. Crosnier, T. Brousse, F. Béguina, Lithium rhenium (VII) oxide as novel material for graphite pre-lithiation in high performance Lithium-ion capacitors. *Journal of Materials Chemistry A*, 2016, (4): 12609-12615.
- [9] K. Leng, F. Zhang, L. Zhang, T. Zhang, Y. Wu, Y. Lu, Y. Huang, Y. Chen, Graphene-based Li-ion hybrid supercapacitors with ultrahigh performance. *Nano Research*, 2013, (6): 581–592.